Available online at www.sciencedirect.com
ScienceDirect
International Journal of Thermal Sciences 45 (2006) 1045–1051
International Journal of Thermal Sciences
www.elsevier.com/locate/ijts

Kinetic modeling of temperature driven flows in short microchannels ☆

Alina A. Alexeenko [a,*], Sergey F. Gimelshein [a], E. Phillip Muntz [a], Andrew D. Ketsdever [b]

[a] *Department of Aerospace and Mechanical Engineering, University of Southern California, Los Angeles, CA 90089, USA*
[b] *Propulsion Directorate, Air Force Research Laboratory, Edwards Air Force Base, CA 93524, USA*

Received 10 September 2005; accepted 23 January 2006

Available online 9 March 2006

Abstract

The temperature driven gas flows in both a two-dimensional finite length microchannel and a cylindrical tube have been studied numerically, with a goal of investigating performance optimization for a nanomembrane-based Knudsen Compressor. The numerical solutions were obtained using the direct simulation Monte Carlo (DSMC) method and a discrete ordinate method for the ellipsoidal statistical and Bhatnagar–Gross–Krook models. The Knudsen number was 0.2 and the length-to-height ratio 5. Three different wall temperature distributions were considered: linear, step-wise, and a non-monotonic profile typical for a radiantly heated Knudsen Compressor's membrane. The short channel end effects are characterized, and the sensitivity of the mass flow to a non-monotonic temperature distribution is shown.

PACS: 47.15.Gf; 47.45.Gx; 47.60.+i; 51.10.+y; 82.20.Wt; 83.50.Ha

Keywords: Kinetic models; Microchannels; Thermal transpiration; BGK; DSMC

1. Introduction

Lab on a chip technology is drawing the attention of scientists from many disciplines. Recent advances in MEMS manufacturing have made it possible to construct microscale analytical sensors such as, integrated gas chromatography systems, miniature optical and mass spectrometers. The miniaturized detection devices will require microscale roughing pumps to provide sensor elements with gas samples at appropriate environmental conditions. A pumping mechanism that can be exploited at microscale is thermal transpiration, a rarefied gas effect that drives gas flows along the temperature gradients in tubes or channels. The main goal of this paper is the numerical study of thermal transpiration flows in short microchannels to aid in the performance optimization of a transpiration based microscale roughing pump known as the Knudsen Compressor [1].

In the early 1900s M. Knudsen [2] built and studied the first transpiration based compressor, consisting of a series of differentially heated and cooled capillaries. Each of the ten stages of the compressor had a capillary section where the wall temperature increased, causing a thermomolecular pressure build-up at the high-temperature end of the capillary. The capillaries were followed by a connector section with a significantly larger cross-sectional area, where the pressure was almost constant and the temperature decreased to its original value at the beginning of the stage. The modern version of Knudsen's experiment was suggested by Pham-Van-Diep et al. [1] and given the name Knudsen Compressor. It was demonstrated by Vargo and Muntz [3]. The most critical element of the Knudsen Compressor developed at USC is the thermal transpiration membrane made of porous materials, such as aerogel, with pore diameters on the order of the mean free path of the gas at standard atmospheric conditions. The temperature gradient is maintained across the transpiration membrane by resistive or radiant heating. Recently, a single-chip, single stage micromachined implementation of a Knudsen pump was reported in Ref. [4], which can evacuate a cavity to 0.46 atm while operating at atmospheric pressure and using 80 mW input power.

☆ This work was supported in part by the US Air Force Office of Scientific Research and the Propulsion Directorate of the Air Force Research Laboratory at Edwards Air Force Base, California. The first author was supported by a USC Women in Science and Engineering Fellowship.
* Corresponding author.
E-mail address: alexeenk@usc.edu (A.A. Alexeenko).

1290-0729/$ – see front matter
doi:10.1016/j.ijthermalsci.2006.01.014

Nomenclature

C	thermal velocity	$\mathrm{m\,s^{-1}}$
f	velocity distribution function	
g	reduced distribution function; relative velocity	
h	channel height	m
Kn	Knudsen number	
L	channel length	m
N	number of molecules in cell	
n	number density	$\mathrm{mol\,m^{-3}}$
p	pressure	Pa
P	quadrature weights	
Pr	Prandtl number	
S	velocity ordinate	
T	temperature	K
U	X-component of velocity	$\mathrm{m\,s^{-1}}$
V	Y-component of velocity	$\mathrm{m\,s^{-1}}$
W	Z-component of velocity	$\mathrm{m\,s^{-1}}$
w	channel width	m

Greek symbols

δ	Kroneker delta	
λ	mean free path	m
μ	viscosity coefficient	$\mathrm{kg\,m^{-1}\,s^{-1}}$
ν	collision frequency	$\mathrm{s^{-1}}$
ϕ	angular ordinate	
ρ	density	$\mathrm{kg\,m^{-3}}$

Subscripts

I	left reservoir
II	right reservoir
δ	discrete velocity
σ	discrete angle

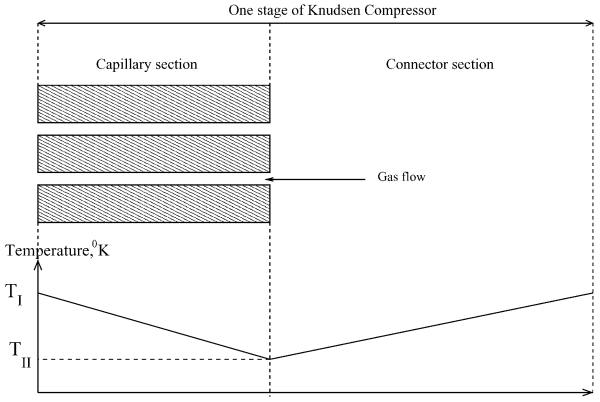

Fig. 1. Schematic of one stage of Knudsen Compressor based on Ref. [19].

The Knudsen Compressor has several attractive features, such as no moving parts and no fluids or lubricants. A schematic of one stage of Knudsen compressor is shown in Fig. 1. There are a number of promising applications provided that its performance can be optimized to meet a variety of pumping requirements. The two most important performance parameters of the compressor are the energy use and device volume per unit throughput. To accomplish minimization of these performance parameters the Knudsen Compressor must also be designed to maximize the gas conductance through the device for a given temperature change. The required flow rate in the Knudsen Compressor can be obtained by adjusting the cross-sectional area of the stages and the temperature distribution along the transpiration membrane at different stages. The main element of the transpiration based pump is rarefied gas flow through a capillary.

Rarefied gas flows of different gases through long tubes and channels have been a topic of extensive experimental and theoretical research over several decades. A comprehensive review of the numerical data and analytical results for rarefied gas flows in capillaries was performed by Sharipov and Seleznev [5] (see also references therein). There is however a lack of reference data for non-isothermal flow through a capillary of a finite length, especially for arbitrary pressure and temperature drops.

The present numerical modeling of thermal transpiration flows in microchannels addresses several questions important for design optimization of Knudsen Compressors. Principally these relate to the influence of different internal temperature distributions across the membrane on the flow field inside the capillaries. The total transpiration mass flows; the impact of rarefaction on the capillary throughput; and capillary end effects are all of interest.

2. Problem statement

In the present work, two reservoirs filled with a single-species gas and joined by a two-dimensional capillary or cylindrical tube, both with a finite length L and height h or radius a, are considered in the computations. The two-dimensional channel configuration corresponds to the case of a capillary of infinite width w. A schematic of the geometric configuration and notations used throughout this paper are shown in Fig. 2. The subscripts I and II refer to the quantities attributed to the left and right container, respectively (far enough from the channel inlet and outlet). The channel walls have some temperature distribution varying from T_I to T_{II}. If the reservoirs are at the same temperature ($T_I = T_{II}$) and the pressure p_I is larger than p_{II} there will be a mass flow from the left container to the right one. Conversely, if the pressures are equal but a temperature drop is maintained between the reservoirs then the gas flow develops from the cold container to the hot one.

The summary of cases that have been considered is given in Table 1. The gas is molecular nitrogen in all simulations. Hereafter, the Knudsen number is based on the mean free path of the gas in the right reservoir and the channel height or tube diameter. Note also that the change in Knudsen number is due to a change in the mean free path and not the capillary geome-

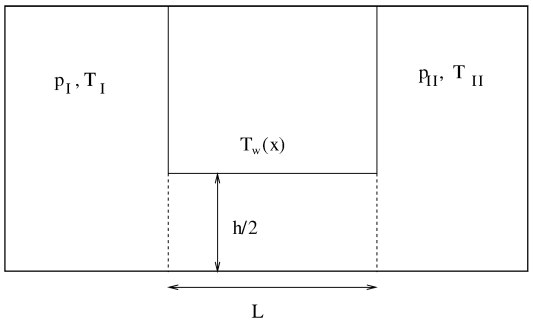

Fig. 2. Schematic of the problem and notations.

Table 1
Summary of cases considered

Flow conditions	Designation
Effect of wall temperature distribution	
Two-dimensional channel:	
$L/h = 5$, $Kn_{II} = 0.2$, N_2, $T_I = 600$ K, $T_{II} = 300$ K, $\frac{p_I}{p_{II}} = 1.0$	
linear	*case* I(a)
step	*case* I(b)
non-monotonic	*case* I(c)
Axisymmetric tube:	
$L/a = 5$, $Kn_{II} = 0.2$, N_2, $T_I = 600$ K, $T_{II} = 300$ K, $\frac{p_I}{p_{II}} = 1.0$	
linear	*case* II(a)
step	*case* II(b)
non-monotonic	*case* II(c)

try. The influence of different wall temperature distributions is examined for a channel and a tube, respectively, that connects reservoirs with a temperature ratio $T_I/T_{II} = 2$ and zero pressure drop. These conditions are typical for the gas flow in the Knudsen Compressor operating with no pressure increase but with maximum flow.

3. DSMC method

The DSMC method [6] has been applied in this work to obtain numerical solutions for short microchannel flows. The DSMC method is a statistical approach for solution of the Boltzmann equation, the governing equation of rarefied flows. The DSMC method, initially proposed by G.A. Bird in the early 1960s, has become the most powerful and accurate method for numerically modeling complex rarefied gas flows [6]. The DSMC-based software SMILE [7] is used for all DSMC computations. The code uses the majorant frequency scheme [8] of the DSMC method for modeling of collisional process. The intermolecular potential is assumed to be the variable soft sphere model [9]. The Larsen–Borgnakke model [10] with temperature-dependent Z_r and Z_v and discrete rotational and vibrational energies is used for the energy exchange between the translational and internal modes. At the gas-wall interface the Maxwell model is used with fully diffuse accommodation of tangential momentum and energy.

The background cell size in 2D DSMC calculations was 1/40th of the channel height, the cell linear dimension is equal to or less than the gas mean free path in all the considered cases. The total number of background cells in each of the considered cases was 96 000. The average number of simulated molecules per background cell was 10. The total number of simulated molecules in the domain was about 1 million.

4. Discrete ordinate method for model kinetic equation

The computational cost of DSMC simulations of low-speed flow in a channel becomes prohibitive due to low signal-to-noise ratio [11]. For modeling of such flows it is reasonable to consider the solution of the steady-state Boltzmann equation with a simplified collision operator,

$$U\frac{\partial f}{\partial x} + V\frac{\partial f}{\partial y} = \nu(f_0 - f) \tag{1}$$

where $f = f(x, y, U, V, W)$ is the distribution function, x and y are Cartesian coordinates, U, V, and W are velocity components, and ν is the collision frequency. For the conventional Bhatnagar–Gross–Krook (BGK) [12] model $f_0 = f_M = n(2\pi RT)^{-3/2}\exp(-\frac{\vec{C}^2}{2RT})$ is the local equilibrium Maxwell–Boltzmann distribution function. For the ellipsoidal statistical (ES) model [13] $f_0 = f_G$ is the local isotropic three-dimensional Gaussian

$$f_G = \frac{n}{\sqrt{(2\pi)^3 \det[\lambda_{ij}]}}\exp(-\epsilon_{ij}c_i c_j)$$
$$\lambda_{ij} = \left(\frac{1}{Pr}\right)RT\delta_{ij} + \frac{1 - 1/Pr}{\rho}p_{ij} \tag{2}$$

where $[\epsilon] = [\lambda]^{-1}$, $\vec{C} = \vec{U} - \vec{\vec{U}}$ is thermal velocity, p_{ij} is the pressure tensor, and Pr is the Prandtl number. If Prandtl number $Pr = 1$ then $f_G = f_M$ and Eq. (1) gives the original BGK model. Eq. (1) is a non-linear integrodifferential equation that uses a simplified form of the collision integral compared to the Boltzmann equation, and is applicable to model gas flows with arbitrary Knudsen numbers and degree of flow nonequilibrium.

The BGK-type model kinetic equation (1) can be solved using a finite-difference method and standard discrete-ordinate method procedures [14,15] for interpolation of the distribution function in velocity space. First, for the two-dimensional problems, reduced distribution functions are introduced:

$$g = \int_{-\infty}^{\infty} f\,\mathrm{d}W, \qquad h = \int_{-\infty}^{\infty} fW^2\,\mathrm{d}W$$

One can introduce the polar coordinates in the velocity space as follows:

$$U = S\sin\phi, \qquad V = S\cos\phi$$

The discrete speeds S_δ and velocity angles ϕ_σ are introduced as the ordinates of the quadratures for the integration of the velocity distribution function. The gas flow parameters are then calculated as

$$n = \sum_{\delta}\sum_{\sigma} P_\delta P_\sigma g_{\delta\sigma}$$

$$nU = \sum_{\delta}\sum_{\sigma} P_\delta P_\sigma S_\delta \sin\phi_\sigma g_{\delta\sigma}$$

$$nV = \sum_{\delta}\sum_{\sigma} P_\delta P_\sigma S_\delta \cos\phi_\sigma g_{\delta\sigma}$$

$$\frac{3}{2}nT = \sum\sum P_\delta P_\sigma \left(h_{\delta\sigma} + S_\delta^2 g_{\delta\sigma}\right)$$

where P_δ, P_σ are quadrature weights. Finally, the resulting system of equations

$$S_\delta \sin\phi_\sigma \frac{\partial g_{\delta\sigma}}{\partial x} + S_\delta \cos\phi_\sigma \frac{\partial g_{\delta\sigma}}{\partial y} = \nu\left(g^0_{\delta\sigma} - g_{\delta\sigma}\right) \tag{3}$$

$$S_\delta \sin\phi_\sigma \frac{\partial h_{\delta\sigma}}{\partial x} + S_\delta \cos\phi_\sigma \frac{\partial h_{\delta\sigma}}{\partial y} = \nu\left(h^0_{\delta\sigma} - h_{\delta\sigma}\right) \tag{4}$$

is solved by the finite-difference method. The Gauss–Hermite half range quadrature [16] of order 16 and three-eighth's rule with 144 ordinates are used for the integration over speed and velocity angle, respectively. The number of grid points in the physical space was 16 671 for the calculations reported in the section below.

5. Results and discussion

Temperature gradient driven flows are very sensitive to thermal boundary conditions. For practical microdevices it is generally difficult to attain idealized thermal boundary requirements. Thus, numerical methods for reliably estimating the magnitude of the consequences induced by non-ideal conditions are important.

As an illustration of the usefulness of this approach consider the recent developments by Young [17] and Han [18] of a prototype Knudsen Compressor. Radiant energy was used to generate temperature gradients in the carbon doped aerogel membranes that are the active elements in the compressor's pumping stages. Due to finite photon mean free paths in the carbon doped aerogel membranes, the wall temperatures in the membrane's flow passages had a maximum near to, but not at, the exit surface of the membrane. This is the motivation for the calculations in this section with the non-monotonic wall temperature variation of case III-c (see Table 1) constructed to mimic the essentials of a membrane in Young's experiments.

The influence of wall temperature distribution on the thermal transpiration flow in short microchannels was considered at $Kn_{II} = 0.2$. To study this effect, the pressure was assumed equal in the two reservoirs, and the temperature drop was set to 300 K. The three cases of temperature distribution are (i) a linear temperature variation along the channel wall (case I-a), (ii) a stepwise temperature variation (case I-b) and (iii) a non-monotonic distribution typical for a radiatively heated nanomembrane Knudsen compressor [17] (case I-c). The non-monotonic wall temperature profile has a maximum of 750 K at one-fourth of the channel length. The three wall temperature distributions are plotted in Fig. 3.

First, the temperature and velocity fields for case I-a calculated by the DSMC method and by the discrete ordinate method

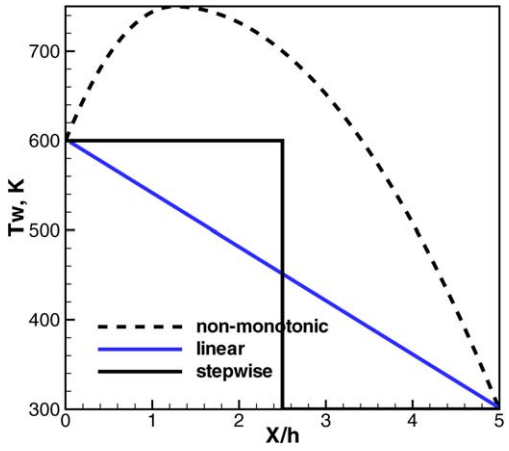

Fig. 3. Wall temperature distributions.

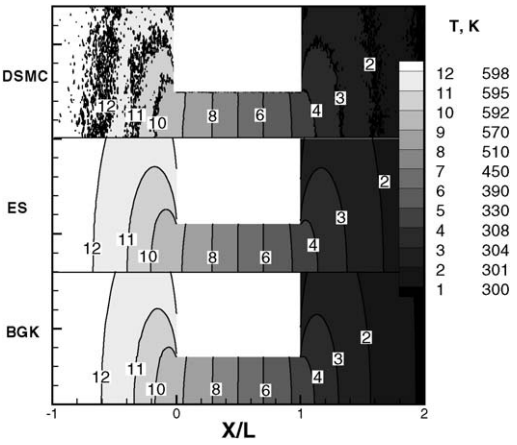

Fig. 4. Translational temperature flow field for case I-a calculated using DSMC (top), ES (center) and BGK (bottom) models.

for BGK and ES models are compared. Translational temperature in the flow field for case I-a is plotted in Fig. 4, calculated by the three methods: DSMC (top), ES (center) and BGK (bottom). All three methods give a very similar predictions of the temperature variation inside the channel and in the upstream and downstream containers.

Figs. 5 and 6 show the comparison of the velocity flowfields and profiles along the X-axis, respectively, calculated by the three models: DSMC, ES and BGK for case I-a. All three methods predict a qualitatively similar flowfield with the velocity increasing in the channel along the temperature gradient from the right reservoir to the left one. However, the streamwise velocity magnitude inside the channel predicted by the BGK model is about 20% lower than that calculated by DSMC and ES. The transpiration velocity is underpredicted by the BGK model because it corresponds to a Prandtl number of 1 instead of the value of around 0.7 typical for diatomic gases at room temperature. This results in an effectively lower coefficient of heat conduction in the BGK solution and smaller values of thermal creep. Figs. 7 and 8 show the streamwise velocity profile along the X-axis for cases I-b and I-c, respectively. Again, the BGK model predicts a significantly lower magnitude of the transpi-

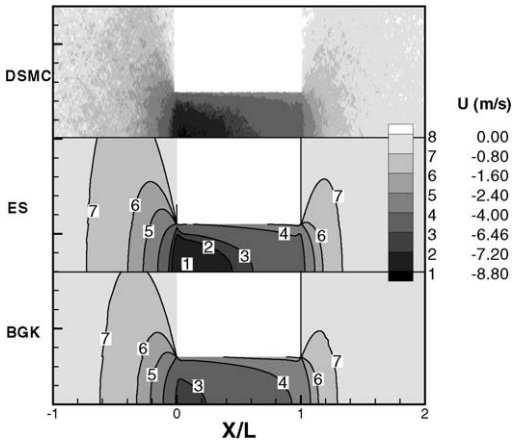

Fig. 5. Streamwise velocity flow field for case I-a calculated using DSMC (top), ES (center) and BGK (bottom) models.

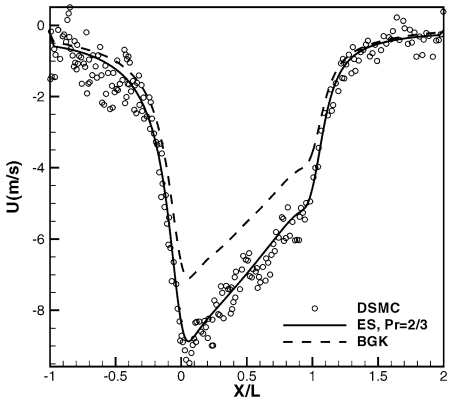

Fig. 6. Streamwise velocity profile along X-axis for case I-a.

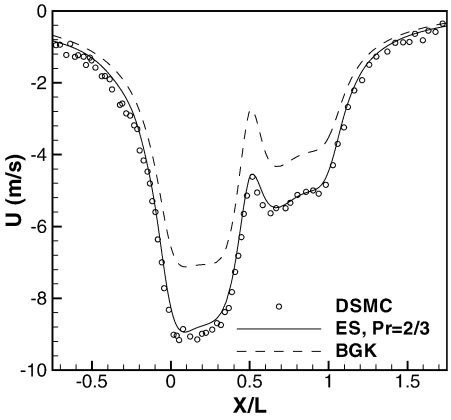

Fig. 7. Streamwise velocity profile along X-axis for case I-b.

ration velocity than the DSMC and ES models. The maximum velocity magnitude at $X = 0$ (channel exit) is about 20% lower for the BGK solution compared to the other two models for all three wall temperature variations.

The DSMC and ES velocity fields show good quantitative agreement with the difference between the two predictions being less than the statistical scatter of the DSMC results. The statistical scatter is inherent in the DSMC results. It is especially

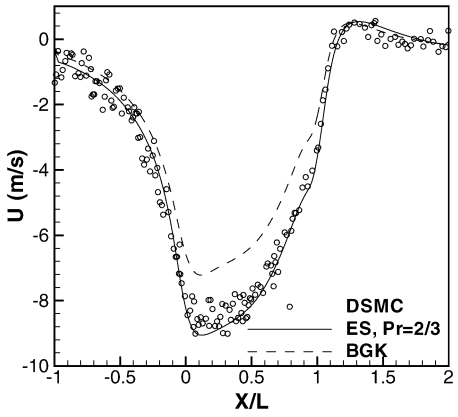

Fig. 8. Streamwise velocity profile along X-axis for case I-c.

pronounced when the average flow velocity is much smaller than the thermal velocity of gas molecules, which is the case for thermal transpiration flows created by a moderate temperature difference. The statistical scatter is inversely proportional to the square root of the sample size in the DSMC. The sample size is equal to the number of time steps used for averaging of the macroparameters times the number of molecules per sampling cell. Therefore, large CPU times are required to obtain a DSMC solution with high signal-to-noise ratio for channel transpiration flows. The CPU time for the DSMC solution in case I-a was about 240 hours using a 2.8 GHz Xenon processor. The CPU time for the ES and BGK solutions was under 8 hours on the same processor. The discrete ordinate method for the ES model kinetic equation can, therefore, provide accurate numerical solutions of transpiration flow in a channel at significantly lower computational cost.

The influence of wall temperature distributions inside the channel on the gas temperature field is illustrated in Fig. 10 where DSMC solutions and ES solutions are plotted at the top and bottom, respectively. The ES and DSMC temperature fields are in good agreement for all of the considered cases of wall temperature distribution. The gas temperature generally follows the surface temperature inside the channel, with the end effects being visible even at a distance from the inlet/outlet equal to the channel length. The end effects are somewhat smaller for the stepwise distribution, and largest for the non-monotonic profile. The change in the wall temperature distribution significantly impacts the flow velocity shown in Fig. 9 where only the ES solutions are given because of the large statistical scatter in the DSMC results.

Fig. 11 shows the pressure profiles along the centerline calculated by the DSMC method for the above temperature distributions. The qualitative behavior is similar for the linear and stepwise distribution, with pressure larger in the hot part, and smaller in the cold part. The non-monotonic case significantly differs from the first two, since there is no significant pressure minimum in the cold part. Also, there is a pressure increase inside the channel of about 10 percent for the monotonic profile due to the reverse transpiration.

The calculated mass flow for the three cases are listed in Table 2. The flow coefficient Q_T is used here that is usually employed for characterization of the thermal creep flows between

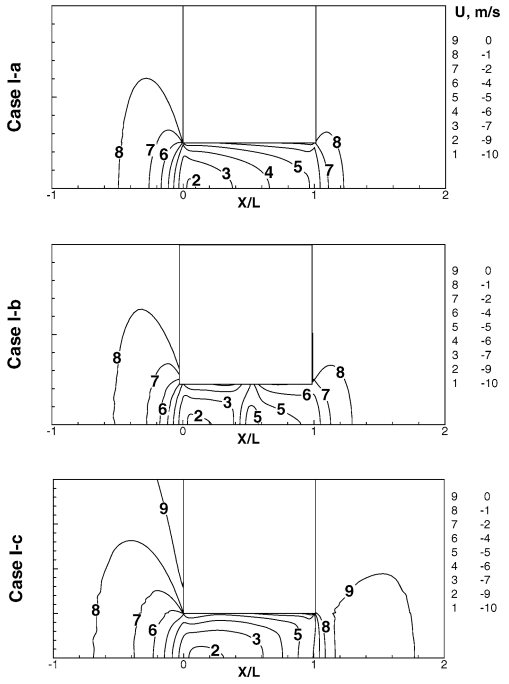

Fig. 9. X-component of velocity fields for different wall temperature distributions: case I-a (top), case I-b (center) and case I-c (bottom). ES solution.

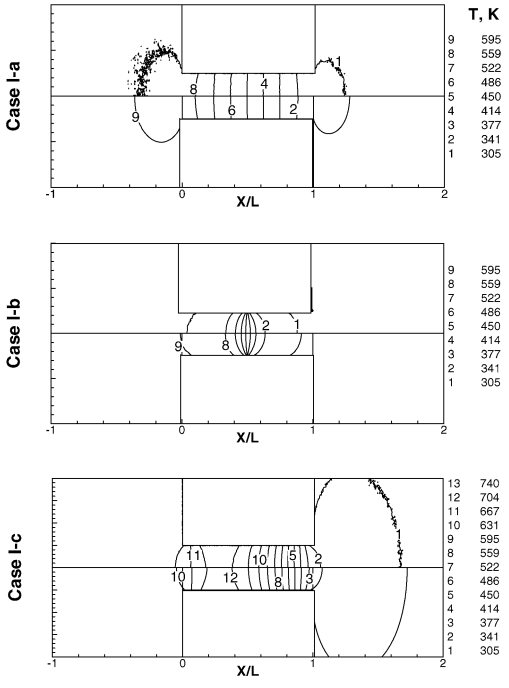

Fig. 10. Translational temperature fields calculated by DSMC (top) and ES (bottom).

parallel plates for the conditions of small temperature and pressure gradients. The flow coefficient is defined as follows:

$$Q_T = \frac{\dot{M}}{(\frac{1}{2}\sqrt{2RT_0})\rho_0 w h^2 \frac{1}{T_0}\frac{\Delta T}{L}} \tag{5}$$

where $\dot{M}$ is the mass flow, ρ_0 and T_0 are the average density and temperature, respectively, and w, h, L are channel width, height and length, respectively.

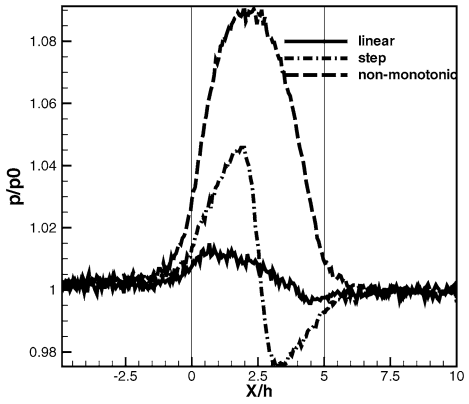

Fig. 11. Pressure profile along the channel, $Kn_H = 0.2$, $L/h = 5$ for different temperature variations, case I. DSMC solution.

Table 2
Calculated flow coefficient for case I

Temperature distribution	DSMC	ES	BGK
linear	0.119	0.117	0.094
stepwise	0.115	0.113	0.087
non-monotonic	0.097	0.099	0.074

Table 3
Calculated flow coefficient Q_T for temperature-driven flow in short tube, case II

Temperature distribution	Q_T
linear	0.1269
stepwise	0.1245
non-monotonic	0.1054

The DSMC and ES model predictions for the mass flow agree to within 2% while the BGK model underestimates the mass flow by about 20% for all considered cases of wall temperature variation. The mass flow in the case of stepwise temperature variation is only slightly lower (by $\approx 3\%$) than for the linear temperature variation. However, the reverse transpiration in the non-monotonic temperature distribution case results in significant degradation of mass throughput (by $\approx 18\%$) for the same temperature difference between the hot and cold containers.

Similar influences of the wall temperature distributions are observed for the cylindrical tube case (see Table 3). The decrease of the mass flow is close to that for a two-dimensional case and is equal to about 2% and 17% for stepwise and non-monotonic wall temperature distributions, respectively.

6. Conclusions

The direct simulation Monte Carlo method and the discrete ordinate method for the solution of the ellipsoidal statistical (ES) and Bhatnagar–Gross–Krook (BGK) models were used to study rarefied gas flow through a two-dimensional, finite length channel. The flow in the transitional regime with a Knudsen number of 0.2 is examined in the presence of temperature gradients. Three different wall temperature distributions were

considered: linear, step-wise, and a non-monotonic profile typical for a radiantly heated Knudsen Compressor's membrane.

The three numerical approaches were compared in terms of flow fields and the mass flow. All three methods gave qualitatively similar flow fields. However, the BGK model significantly, by 20%, underpredicts the transpiration velocity and flow coefficient, whereas the ES model and the benchmark DSMC method predictions are in good quantitative agreement throughout the whole computational domain. The discrete ordinate method for the ellipsoidal statistical model kinetic equation provides accurate numerical solutions of transpiration flow in a channel at a significantly lower computational cost compared to the DSMC method.

The influence of several wall temperature distribution on the thermal transpiration flow in a short channel was considered. The non-monotonic wall temperature distribution case significantly differs from the linear and stepwise ones. There is a pressure increase inside the channel of about 10 percent for the non-monotonic profile due to reverse transpiration. The mass flow in case of the stepwise temperature variation is only slightly lower (by 3%) than for the linear temperature variation. However, the reverse transpiration caused by the non-monotonic wall temperature distribution results in significant degradation of mass flow, by about 18% for the same temperature difference between the hot and cold container. Similar influences of the wall temperature distributions have been obtained for a cylindrical tube case.

The application of the numerical simulations based on the ellipsoidal statistical model discussed in this paper to detailed investigations and optimizations of microscale thermal creep flows will be extremely valuable. The work reported here is a first look at describing practical thermal gradient driven flows in Knudsen Compressors. While the available results are at present relatively scarce, they do validate the ES model in this application. Useful quantitative estimates have been obtained for the consequences of the particular wall temperature profiles chosen for the calculations.

References

[1] G. Pham-Van-Diep, P. Keeley, E.P. Muntz, D.P. Weaver, A micromechanical Knudsen compressor, in: J. Harvey, G. Lord (Eds.), Rarefied Gas Dynamics, Oxford University Press, Oxford, 1995, pp. 715–721.

[2] M. Knudsen, Eine Revision der Gleichgewichtsbedingung der Gase: Thermische Molekularströmung, Ann. Phys., Leipzig 31 (1910) 205–229.

[3] S.E. Vargo, E.P. Muntz, An evaluation of a multiple stage micromechanical Knudsen compressor and vacuum pump, in: Ching Shen (Ed.), Rarefied Gas Dynamics, Peking University Press, Beijing, 1997, pp. 995–1000.

[4] S. McNamara, Y.B. Gianchandani, A micromachined Knudsen pump for on-chip vacuum, in: Proceedings of the 12th International Conference on Solid State Sensors, Actuator and Microsystems, Boston, MA, vol. 2, 2003, pp. 1919–1922.

[5] F. Sharipov, V. Seleznev, Data on internal rarefied gas flows, J. Phys. Chem. Ref. Data 27 (3) (1998) 657–706.

[6] G.A. Bird, Molecular Gas Dynamics and the Direct Simulation of Gas Flows, Clarendon Press, Oxford, 1994.

[7] M.S. Ivanov, G.N. Markelov, S.F. Gimelshein, Statistical simulation of reactive rarefied flows: Numerical approach and applications, AIAA Paper 98-2669.

[8] M.S. Ivanov, S.V. Rogasinsky, Analysis of numerical techniques of the direct simulation Monte Carlo method in the rarefied gas dynamics, Sov. J. Numer. Anal. Math. Modeling 3 (6) (1988) 453–465.

[9] K. Koura, H. Matsumoto, Variable soft sphere molecular model for inverse-power-law of Lennard-Jones potential, Phys. Fluids A 3 (10) (1991) 2459–2465.

[10] C. Borgnakke, P.S. Larsen, Statistical collision model for Monte Carlo simulation of polyatomic gas mixture, J. Comput. Phys. 18 (1975) 405–420.

[11] C. Cai, D. Boyd, I.J. Fan, G.V. Candler, Direct simulation methods for low-speed microchannel flow, J. Thermophysics Heat Transfer 14 (3) (2000) 368–378.

[12] P.L. Bhatnagar, E.P. Gross, M. Krook, A model for collision processes in gases. I. small amplitude processes in charged and neutral one-component systems, Phys. Rev. 94 (3) (1954) 511–525.

[13] P. Andries, P.L. Tallec, J.P. Perlat, B. Perthame, The Gaussian-bgk model of Boltzmann equation with small Prandtl number, European J. Mech. B Fluids 19 (2000) 813–830.

[14] C. Cercignani, Theory and Application of the Boltzmann Equation, Elsevier, New York, 1975.

[15] C. Chung, S. Wereley, Numerical analysis of low-speed gas flows in microchannels, AIAA Paper 2003-860.

[16] B. Shizgal, A Gaussian quadrature procedure for use in the solution of the Boltzmann equation and related problems, J. Comput. Phys. 41 (1981) 309–328.

[17] M. Young, Investigation of several important phenomena associated with the development of Knudsen Compressors, PhD thesis, University of Southern California, 2004.

[18] Y.L. Han, Investigation of Knudsen Compressors at low pressures, PhD thesis, University of Southern California, 2005.

[19] E.P. Muntz, Y. Sone, K. Aoki, S. Vargo, M. Young, Performance analysis and optimization considerations for a Knudsen Compressor in transitional flow, J. Vac. Sci. Technol. A 20 (1) (2002) 214–224.